Am J Nucl Med Mol Imaging 2020;10(1):57-65
www.ajnmmi.us /ISSN:2160-8407/ajnmmi0102852

Original Article

Assessing bladder hyper-permeability biomarkers *in vivo* using molecularly-targeted MRI

Rheal A Towner[1,2], Nataliya Smith[1], Debra Saunders[1], Megan Lerner[3], Beverley Greenwood-Van Meerveld[4], Robert E Hurst[5]

[1]Advanced Magnetic Resonance Center, Oklahoma Medical Research Foundation, Oklahoma, OK, USA; Departments of [2]Pathology, [3]Surgery Research Laboratory, [4]Physiology, [5]Urology, University of Oklahoma Health Sciences Center, Oklahoma, OK, USA

Received September 26, 2019; Accepted February 21, 2020; Epub February 25, 2020; Published February 28, 2020

Abstract: The objective was to investigate if some of the key molecular players associated with bladder hyper-permeability in interstitial cystitis/bladder pain syndrome (IC/BPS) could be visualized with molecularly-targeted magnetic resonance imaging (mt-MRI) *in vivo*. IC/BPS is a chronic, painful condition of the bladder that affects primarily women. It has been demonstrated over the past several decades that permeability plays a substantial role in IC/BPS. There are several key molecular markers that have been associated with permeability, including glycolsaminoglycan (GAG), biglycan, chondroitin sulfate, decorin, E-cadherin, keratin 20, uroplakin, vascular endothelial growth factor receptor 1 (VEGF-R1), claudin-2 and zonula occludens-1 (ZO-1). We used *in vivo* molecularly-targeted MRI (mt-MRI) to assess specific urothelial biomarkers (decorin, VEGF-R1, and claudin-2) associated with bladder hyper-permeability in a protamine sulfate (PS)-induced rat model. The mt-MRI probes consisted of an antibody against either VEGF-R1, decorin or claudin-2 conjugated to albumin that had also Gd-DTPA (gadolinium diethylene triamine penta acetic acid) and biotin attached. mt-MRI- and histologically-detectable levels of decorin and VEGF-R1 were both found to decrease following PS-induced bladder urothelial hyper-permeability, whereas claudin-2, was found to increase in the rat PS model. Verification of the presence of the mt-MRI probes were done by targeting the biotin moiety for each respective probe with streptavidin-hose radish peroxidase (HRP). Levels of protein expression for VEGF-R1, decorin and claudin-2 were confirmed with immunohistochemistry. *In vivo* molecularly-targeted MRI (mt-MRI) was found to successfully detect alterations in the expression of decorin, VEGFR1 and claudin-2 in a PS-induced rat bladder permeability model. This *in vivo* molecularly-targeted imaging approach has the potential to provide invaluable information to enhance our understanding of bladder urothelium hyper-permeability in IC/BPS patients, and perhaps be used to assist in developing novel therapeutic strategies.

Keywords: Claudin-2, vascular endothelial growth factor receptor 1 (VEGF-R1), decorin, molecularly-targeted magnetic resonance imaging (mt-MRI), interstitial cystitis (IC), in vivo, protamine sulfate (PS), rats, intravesical

Introduction

Interstitial cystitis/bladder pain syndrome (IC/BPS) is a chronic, painful condition of the bladder that affects up to 7% of females in the U.S.A. [1], and is associated with a significant minority (>30%) of female patients with chronic pelvic pain [2]. The prevalence of IC/BPS is markedly higher (100-300/100,000 women) than previously thought [3]. Frequency, urgency and pain during bladder filling are the most commonly reported symptoms of IC/BPS [4]. IC/BPS is thought to be either a type of hypersensitivity disorder that affects bladder and other somatic/visceral organs with many overlapping symptoms and pathophysiology, or a continuum of painful vs. non-painful overactive bladder syndrome [5].

Not only is the etiology of IC/BPS unknown, but there is considerable debate as to whether it occurs due to events within or from outside the bladder, or whether both occur. What is currently known is that permeability does play a role. Parsons has long argued that a key etiologic factor involves permeability that is produced by loss of the glycosaminoglycan (GAG) layer that he argues is a major component of the bladder

defenses that produce impermeability [6-15]. Parsons demonstrated increased uptake of instilled urea from the bladders of IC patients [16], and Buffington showed altered excretion of injected fluorescein, presumably representing recycling of the dye in the urine [17]. We also recently used contrast-enhanced MRI to directly measure bladder permeability in IC patients [18]. Increased permeability was thought to result in pain from the same mechanism as produces pain in bladder cancer, CIS, and infection, namely loss of the specialized "umbrella" cells that form the luminal layer of cells and are responsible for maintaining the impermeability barrier. Impermeability is maintained by multiple "defense molecules" [19], tight junctions [20] and the uroplakin plaques [21], and also the GAG layer [22].

Uroplakin [19, 23-25], keratin 20 [23, 26], chondroitin sulfate [23, 27-29], decorin [23, 30], VEGF-R1 [31, 32], and claudin-2 [33] are all known bladder urothelium markers. In feline interstitial cystitis, which is thought to emulate human IC/BPS, there were definite changes in luminal GAG observed, as well as several altered protein expressions [23]. Abnormalities in protein expression included biglycan, chondroitin sulfate, decorin, E-cadherin, keratin, uroplakin and ZO-1 [23]. In particular, chondroitin sulfate, biglycan and decorin levels were substantially low in expression [23].

Intravesical administration of Gd-DTPA in conjunction with the use of dynamic CE-MRI (DCE-MRI) was developed by our group and validated in a rat pre-clinical model as well as in a small cohort of IC patients. We developed an *in vivo* MRI test to assess increased bladder urothelial permeability in a pre-clinical rat model following protamine sulfate (PS) exposure using a dynamic contrast-enhanced magnetic resonance imaging (DCE-MRI) approach [34]. This method involves intravesical administration of a contrast agent, Gd-DTPA, to monitor leakage or uptake of this agent through the bladder wall. The enhanced contrast MR imaging approach was found to detect bladder urothelium leakage of the contrast agent in rat bladder urothelial [34]. The CE-MRI approach can also be used to assess the effect of therapeutic intervention regarding decreased bladder urothelium permeability. The advantage of the DCE-MRI approach is that 2D and 3D regions of the bladder urothelium can be assessed to establish if there are areas of the bladder wall that are more susceptible to bladder permeability alterations. Gd-DTPA MRI contrast agent was also taken up and significantly retained in human IC bladder urothelium, compared to normal control bladders [18], and that this method could potentially be used as a diagnostic tool to help evaluate bladder hyper-permeability alterations in IC patients. The agent was well tolerated by all IC patients tested, indicating this technology could be translated rapidly to the clinic.

We wanted to investigate if some of the key molecular players associated with bladder hyperpermeability could be visualized with molecularly-targeted MRI. In this study, we used *in vivo* molecular-targeted MRI to assess specific urothelial biomarkers (decorin, VEGF-R1, and claudin-2) associated with bladder permeability alterations in a protamine sulfate (PS)-induced rat model for bladder hyper-permeability.

Materials and methods

Animals

All experiments involving animals was approved by the Oklahoma Medical Research Foundation (OMRF) Institutional Animal Care and Use Committee (IACUC), and followed the National Research Council guide for the care and use of laboratory animals. Female rats (ovarectimized (OVX)) (200-250 g) were anesthetized with isoflurane (1.5-3.0% with 800-1,000 mL O_2) for MRI experiments. PS was administered at a concentration of 1 mg/mL (in saline) in a total volume of 800 μL via an intravesical catheter. A lubricated sterile catheter (18 gauge) was used to transurethally catheterize each animal. PS was instilled in the bladder for 10 min. PS was then removed from the bladder using abdominal pressure and followed by 3 saline flushes (400 μL per flush). Bladder permeability assessments were made at 24 hr following exposure to PS (n=4 for each mt-MRI group). Sham controls (n=4) were administered saline (800 μL) instead of PS.

Molecular-targeted MR imaging probes

Specific probes were synthesized by coupling antibodies against each biomarker to albumin in the Gd-DTPA-albumin-biotin construct. We have previously used this approach for mole-

cularly-targeted MRI probes for *in vivo* VEGF-R2 [35, 36], iNOS [37] and free radical [38-43] detection. The macromolecular contrast material, biotin-BSA-Gd-DTPA, was prepared using a modification of the method of Dafni *et al*. [44]. The biotin moiety in the contrast material was added to allow histological localization. Biotin-BSA-Gd-DTPA was synthesized as described in Coutinho de Souza et al. [40]. A solution of biotin-BSA-Gd-DTPA was added directly to the solution of antibody (anti-DMPO, 200 μg/mL) for conjugation through a sulfo-NHS (N-succinimidyl-S-acetylthioacetate)-EDC (N-succinimidyl 3-(2-pyridyldithio)-propionate) link between albumin and antibody according to the protocol of Hermanson [45]. Sulfo-NHS was added to the solution of biotin-BSA-Gd-DTPA and EDC. This activated solution was added directly to the antibody (anti-DMPO, 200 μg/mL) for conjugation. The mixture was left to react for at least 2 h at 25°C in the dark. The product was lyophilized and subsequently stored at 4°C and reconstituted to the desired concentration for injections in phosphate buffer saline (PBS). Each probe (0.1 mg/kg bw; 200 μL diluted in saline for 800 μl total volume) was administered via an intravesical catheter, instilled for an hour, and flushed with saline. For decorin-targeted, VEGF-R1-targeted or claudin-2-targeted molecular MRI, rats (PS-treated, or their respective shams) were administered either a biotin-Gd-DTPA-albumin-anti-decorin (anti-decorin) probe, a biotin-Gd-DTPA-albumin-anti-VEGF-R1 (anti-VEGF-R1 probe), or a biotin-Gd-DTPA-albumin-anti-claudin-2 (anti-claudin-2 probe) (i.v.; 1 mg/kg in 800 μL, and scanned at pre-contrast, and 4 hours post-targeted contrast agents (anti-decorin, anti-VEGF-R1, or anti-claudin-2 probes).

Magnetic resonance imaging (MRI)

MRI experiments were conducted on a 7 Tesla 30 cm-bore Bruker Biospec MRI system. A RARE (Rapid acquisition with relaxation enhancement) variable TR sequence was used to detect changes in MRI signal intensities and T_1 relaxation maps using a TR (repetition time) =200, 400, 800, 1200 and 1600 ms, TE (echo time) =15 ms, 20 transverse 1 mm-thick slices, a field of view of 3.5 × 3.5 cm^2, matrix 256 × 256, with an in-plane resolution of 137 × 137 μm^2 (as previously done [35-43]) resulting from the administration of the molecular-targeted MRI probes. Pre- and post-probe administration images were taken to establish specific uptake of each probe in the bladder urothelium.

MRI analysis

MRI signal intensities and T_1 values were measured from regions-of-interest (ROIs) within images (ROIs were taken in bladder walls from images and T_1 maps, along with corresponding regions in sham animal datasets, as displayed on Paravision (v 5.0, Bruker Biospin)).

Histology and immunohistochemistry (IHC)

Ex vivo bladder urothelium tissue samples, utilizing MRI coordinates from the MR images, were assessed by histology and immunohistochemistry (IHC) to characterize which bladder urothelium markers were altered. Quantification of IHC markers was done using an Aperio ScanScope Image Analysis System [46]. The bladders of each animal were removed, preserved in 10% neutral buffered formalin, and processed routinely. Hematoxylin-eosin staining: tissues were fixed in 10% neutral buffered formalin, dehydrated, and embedded in paraffin. Sections were deparaffinized, rehydrated, and stained according to standard protocols. Several reagents were produced by Vector Labs Inc. (VLI) in Burlingame, CA. Histological sections (5 μm) embedded in paraffin and mounted on HistoBond® Plus slides (Statlab Medical Products, Lewisville, TX) were rehydrated and washed in Phosphate Buffered Saline (PBS). The sections were processed using the ImmPRESS™ VR Reagent Anti-Rabbit IgG Peroxidase (VLI cat #MP-6401). Antigen retrieval (pH 6 citrate antigen unmasking solution; (VLI cat#H-3300) was accomplished via 20-minutes in a steamer followed by 30-minutes cooling at room temperature. Sections were treated with a peroxidase blocking reagent (Bloxall, VLI cat#SP-6000), followed by 2.5% normal horse serum to inhibit nonspecific binding. Anti-claudin-2, anti-VEGFR1, or anti-decorin antibodies (Invitrogen, ThermoFisher Scientific, Waltham, MA) were separately applied to each section, from bladders not undergoing mt-MRI (n=5/group × 2 groups; saline vs. PS), and following incubation overnight (4°C) in a humidified chamber, sections were washed in PBS, the ImmPRESS VR reagent was applied according to the manufacturer's directions. Sections for streptavidin horse radish peroxidase (SA-HRP), for the bladders that underwent mt-MRI (n=5/

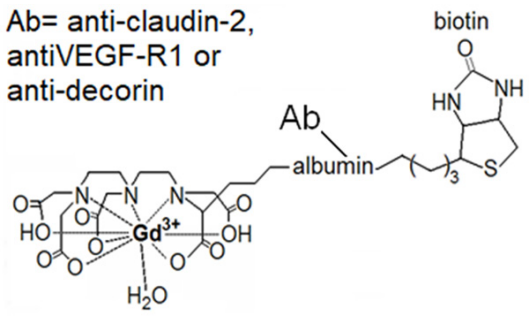

Figure 1. Illustration of the Gd-DTPA-albumin-Ab-biotin probe construct used to generate anti-claudin-2, anti-VEF-R1, and anti-decorin probes.

group × 2 groups; saline vs. LPS), where the streptavidin targets the biotin moiety of the mt-MRI probes, were processed as above, except they were incubated overnight with ready to use (RTU) Strp-HRP (VLI cat#SA-5704). Appropriate washes were in PBS. Slides were incubated with NovaRed® (VLI cat#SK-4805) chromogen for visualization. Counterstaining was carried out with Hematoxylin QS Nuclear Counterstain (VLI). Appropriate positive and negative tissue controls were used.

Statistical analysis

Levels of the molecular-targeted MRI imaging probes were compared between PS- or saline-treated rats, using bivariate correlation coefficients. Data analyses used IBM SPSS Statistics (IBM Corp. Released 2011. IBM SPSS Statistics for Windows, Version 20.0. Armonk, NY: IBM Corp). *P*-values <0.05 were considered significant.

Results

Figure 1 is an illustration of the molecularly-targeted probes used to assess levels of claudin-2, VEGF-R1 and decorin. **Figures 2**-**4** indicates the feasibility of conducting *in vivo* molecular-targeted MR imaging for bladder permeability biomarkers claudin-2 (**Figure 2**), VEGF-R1 (**Figure 3**) and decorin (**Figure 4**), in PS-exposed rat bladders, respectively. Claudin-2 levels are significantly increased (P<0.05) in PS-treated rat bladders (**Figure 2A**, **2C**), compared to saline controls (n=4/group), which had low levels (**Figure 2B**, **2C**). Streptavidin-horse radish peroxidase (SA-HRP) was used to target the anti-claudin-2 probe in PS-(**Figure 2D**) and saline-(**Figure 2E**)-treated rat bladders. Note the higher detection of the anti-claudin-2 probe in the PS-treated rat bladder, compared to the saline-treated bladder. Conversely, VEGF-R1 and decorin levels were significantly lower in PS-treated rat bladders (n=4/group; P<0.01 and P<0.05, respectively) compared to controls (n=4 for both; **Figures 3** and **4**, respectively). Note low levels of both VEGF-R1 and decorin in the bladder dome regions (**Figures 3Bii** and **4Bii**, respectively). SA-HRP was used to target the anti-VEGF-R1 probe in saline-(**Figure 3D**) and PS-(**Figure 3E**)-treated rat bladders. Note the higher detection of the anti-VEGF-R1 probe in the saline-treated rat bladder, compared to the PS-treated bladder. SA-HRP was used to target the anti-decorin probe in saline-(**Figure 4D**) and PS-(**Figure 4E**)-treated rat bladders. Note the higher detection of the anti-decorin probe in the saline-treated rat bladder, compared to the PS-treated bladder. SA-HRP was used to target the biotin moiety of each probe in *ex vivo* tissues, which supported the *in vivo* data.

Confirmation of IHC levels of each biomarker were also obtained from ex vivo rat bladder sections. **Figure 5** depicts levels of claudin-2, VEGF-R1 and decorin in either saline- or PS-treated rat bladders. Note the higher level of claudin-2 staining in the PS-treated rat bladder, compared to the saline control. Note the higher levels of both VEGF-R1 and decorin in the saline control bladders, compared to the PS-treated bladders.

Discussion

A Gd-DTPA-albumin-biotin construct (as previously used by our group [38-43]) was used to conjugate an antibody against specific permeability biomarkers to the albumin moiety. In a previous study using a similar Gd-DTPA-albumin-biotin construct with another antibody to detect macromolecular free radicals, we were able to detect ~0.5-1.0 × 10^{-4} M concentration of the molecularly-targeted probe [38], indicating sensitivity in the micromolar range. From T_1 values, estimation of the anti-decorin probe concentration ranges detected were ~0.7-3.0 × 10^{-4} M, ~0.8-5.0 × 10^{-4} M for the anti-VEGF-R1 probe, and ~0.2-1.0 × 10^{-4} M for the anti-claudin-2 probe. The advantage of this construct involves not only assessing in vivo molecular expression assessment of pertinent biomarkers, but also allows direct ex vivo tissue confir-

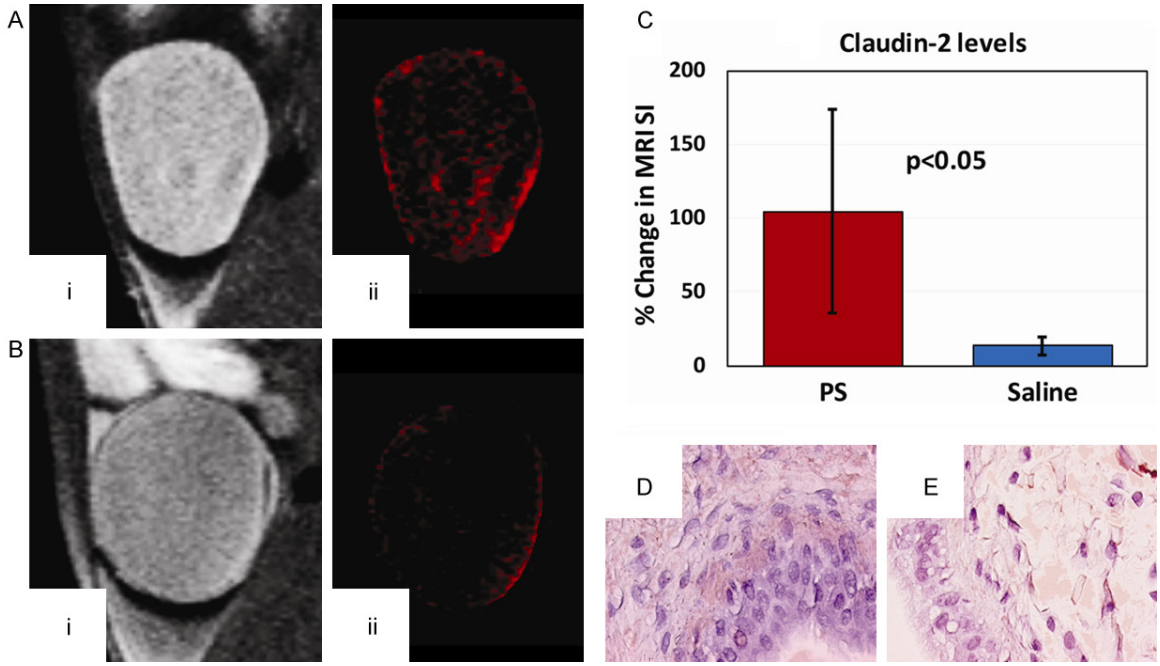

Figure 2. In vivo molecular-targeted MRI of claudin-2 in (A) PS- and (B) sa-line-treated rat bladders (24 h). (ii) Color-enhanced image. (C) Percent change in MRI signal intensities (SI). Significant increase in % MRI SI in PS vs. saline bladders ($P<0.05$). Streptavidin-HRP targeting biotin moiety of probe in (D) PS- or (E) saline-treated bladders.

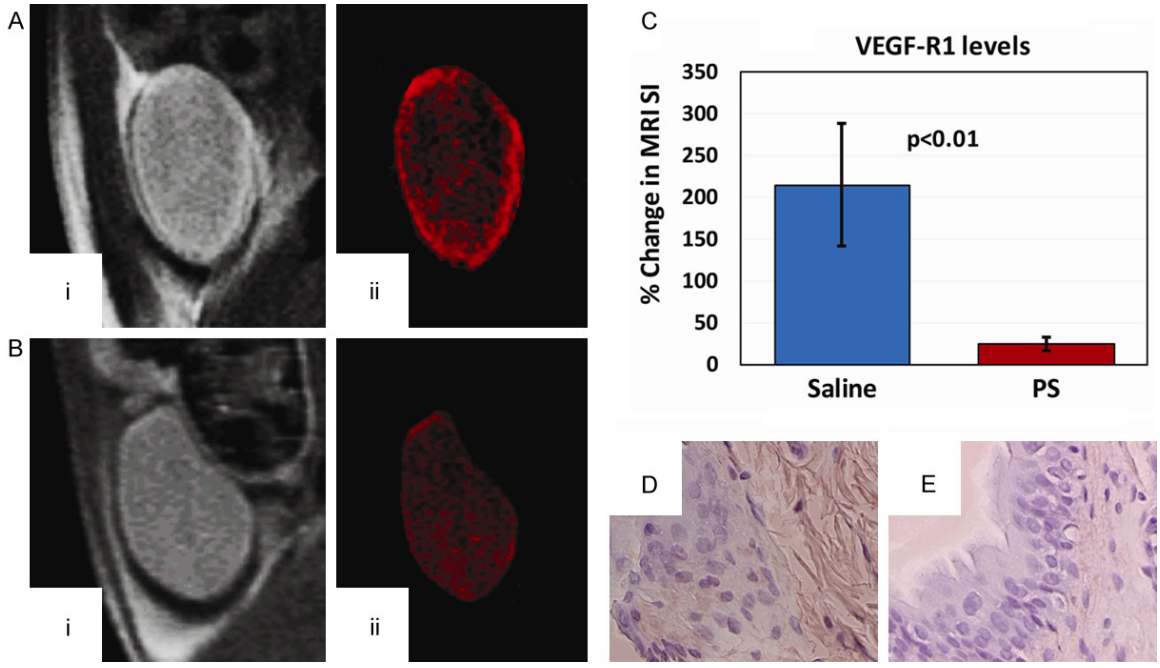

Figure 3. In vivo molecular-targeted MRI of VEGF-R1 in (A) saline- and (B) PS-treated rat bladders (24 h). (ii) Color-enhanced image. (C) Percent change in MRI signal intensities (SI). Significant increase in % MRI SI in saline vs. PS bladders ($P<0.01$). Streptavidin-HRP targeting biotin moiety of probe in (D) saline- or (E) PS-treated bladders.

mation regarding whether the molecular imaging probe reached its' intended target. The conjugates were tested in a rat model of permeability in which brief treatment (10 min) with

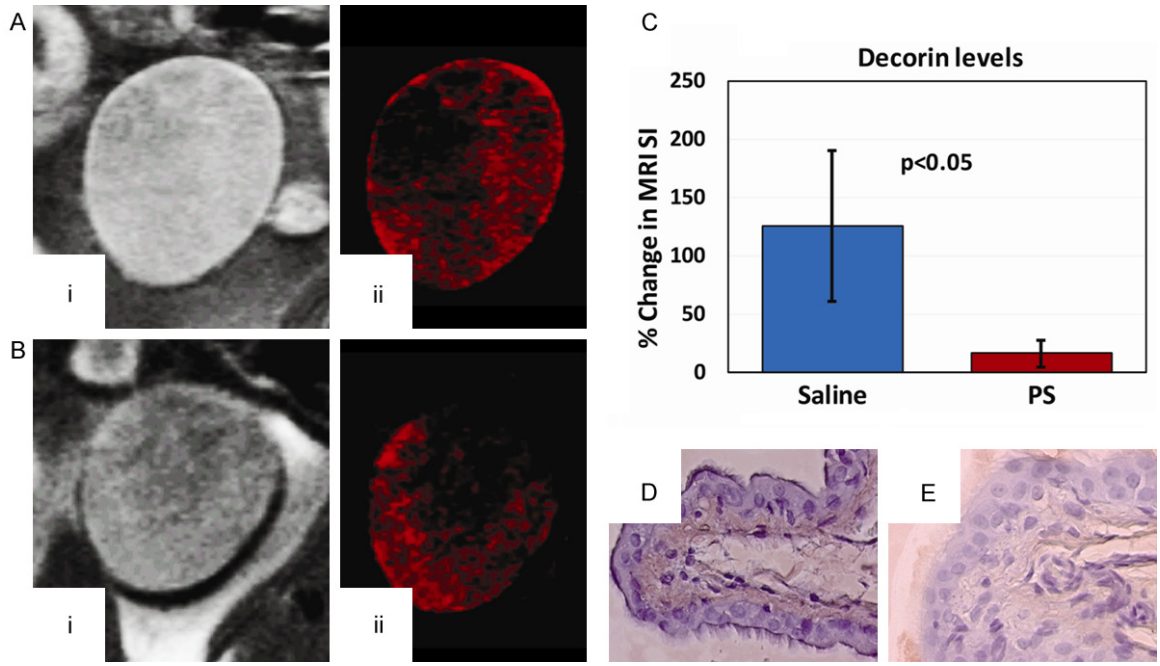

Figure 4. In vivo molecular-targeted MRI of decorin in (A) saline- and (B) PS-treated rat bladders (24 h). (ii) Color-enhanced image. (C) Percent change in MRI signal intensities (SI). Significant increase in % MRI SI in saline vs. PS bladders ($P<0.05$). Streptavidin-HRP targeting biotin moiety of probe in (D) saline- or (E) PS-treated bladders.

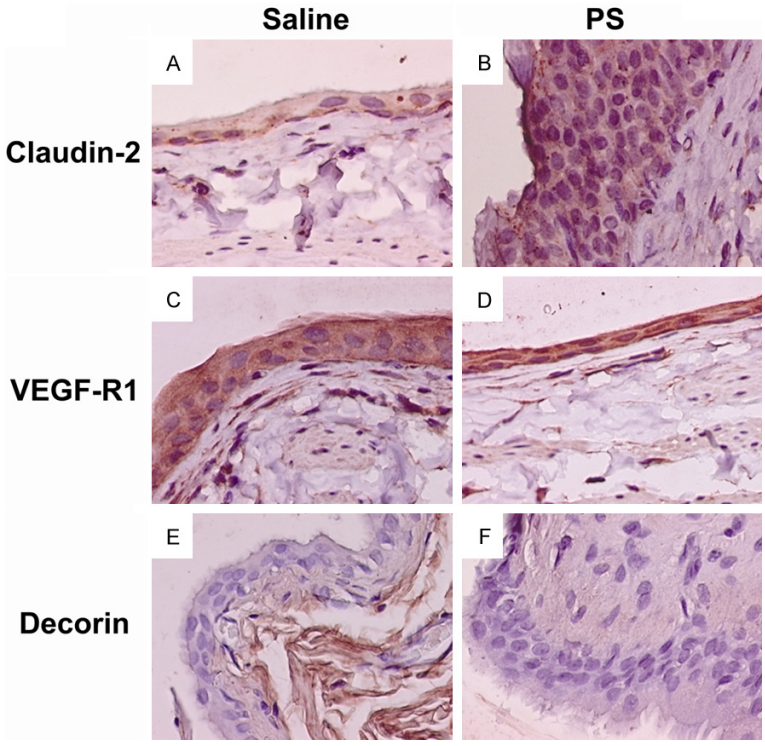

Figure 5. Ex vivo immunohistochemistry (IHC) staining for claudin-2, VEGF-R1 and decorin. Saline-treated rat bladders (A: Claudin-2; C: VEGF-R1; and E: Decorin). Protamine sulfate (PS)-treated rat bladders (B: Claudin-2; D: VEGF-R1; and F: Decorin).

dilute PS (1 mg/ml) is used to induce permeability in the bladder without producing sloughing of the luminal cell layer [34].

Decorin [23, 30], VEGF-R1 [31, 32], and claudin-2 [33] have been well documented as well-known bladder urothelium markers. Most of these bladder urothelium markers were previously identified by our group (Hurst and co-workers) [19, 23, 27], and correlated with histology and immunohistochemistry. VEGF-R1 has been previously found as an integral growth factor that stimulates embryonic urinary bladder development [47]. Relevant to IC patients, VEGF-R1 is significantly down-regulated [31]. Decorin, a proteoglycan of chondroitin/dermatan sulfate, has been found to also decrease in feline IC, which is thought to be similar to hu-

man IC [23]. On the other hand, claudin-2 has been well documented to increase in cystitis [33, 48-50].

Decorin and VEGF-R1 are both expected to decrease (negative response) in PS-induced rat bladders, compared to saline controls, whereas claudin-2 is expected to increase (positive response), compared to saline controls. These observed alterations were supported by the mt-MRI and histological data. MRI- and histologically-detectable levels of decorin and VEGF-R1 were both found to decrease following PS-induced bladder urothelial hyper-permeability. Claudin-2, on the other hand, is over-expressed in relationship to bladder wall hyper-permeability, and was found to increase in the PS model.

Understanding the molecular changes in human patient bladders in IC/BPS has been difficult to achieve because of the necessity of obtaining biopsies for labeling studies. Moreover, evidence from feline bladders suggests that changes in marker distribution may not be uniform over the whole bladder with areas of normal expression coexisting with areas of aberrant expression [23]. This MRI technique should allow more accurate determination of altered biomarker expression in patients that takes spatial distribution into account. Not only can MRI assess the permeability of patient bladders, but also by using molecularly targeted probes, a picture of the molecular changes in defense molecules can be assessed. With these capabilities, better classification of patients and diagnosis should be possible.

In vivo molecularly-targeted MRI (mt-MRI) was found to successfully detect alterations in the expression of decorin, VEGFR1 and claudin-2 in a PS-induced rat bladder permeability model. This in vivo molecular imaging approach can provide invaluable information regarding enhancing our understanding associated with bladder urothelium hyper-permeability in IC patients, and perhaps be used to assist in developing therapeutic strategies.

Acknowledgements

Funding was provided by the Presbyterian Health Foundation (RAT).

Disclosure of conflict of interest

None.

Address correspondence to: Dr. Rheal A Towner, Advanced Magnetic Resonance Center, Oklahoma Medical Research Foundation, 825 NE 13th Street, Oklahoma, OK, USA. Tel: 405-271-7383; E-mail: Rheal-Towner@omrf.org

References

[1] Berry SH, Elliott MN, Suttorp M, Bogart LM, Stoto MA, Eggers P, Nyberg L and Clemens JQ. Prevalence of symptoms of bladder pain syndrome/interstitial cystitis among adult females in the United States. J Urol 2011; 186: 540-4.

[2] Cervigni M and Natale F. Gynecological disorders in bladder pain syndrome/interstitial cystitis patients. Int J Urol 2014; 21 Suppl 1: 85-8.

[3] Chrysanthopoulou EL and Doumouchtsis SK. Challenges and current evidence on the management of bladder pain syndrome. Neurol Urodyn 2013; 33: 1193-201.

[4] Offiah I, McMahon SB and O'Reilly BA. Interstitial cystitis/bladder pain syndrome: diagnosis and management. Int Urogynecol J 2013; 24: 1243-56.

[5] Hanno PM, Erickson D, Moldwin R and Faraday MM; American Urological Association. Diagnosis and treatment of interstitial cystitis/bladder pain syndrome: AUA guideline amendment. J Urol 2015; 193: 1545-53.

[6] Parsons CL, Stauffer C and Schmidt JD. Bladder-surface glycosaminoglycans: an efficient mechanism of environmental adaptation. Science 1980; 208: 605-7.

[7] Parsons CL, Schmidt JD and Pollen JJ. Successful treatment of interstitial cystitis with sodium pentosanpolysulfate. J Urol 1983; 130: 51-3.

[8] Parsons CL. Bladder surface glycosaminoglycan: efficient mechanism of environmental adaptation. Urology 1986; 27: 9-14.

[9] Parsons CL and Mulholland SG. Successful therapy of interstitial cystitis with pentosanpolysulfate. J Urol 1987; 138: 513-6.

[10] Lilly JD and Parsons CL. Bladder surface glycosaminoglycans is a human epithelial permeability barrier. Surg Gynecol Obstet 1990; 171: 493-6.

[11] Parsons CL, Boychuk D, Jones S, Hurst RE and Callahan H. Bladder surface glycosaminoglycans: an epithelial permeability barrier. J Urol 1990; 143: 139-42.

[12] Parsons CL. A model for the function of glycosaminoglycans in the urinary tract. World J Urol 1994; 12: 38-42.

[13] Parsons CL. The role of the urinary epithelium in the pathogenesis of interstitial cystitis/prostatitis/urethritis. Urology 2007; 69: 9-16.

[14] Parsons CL. The role of a leaky epithelium and potassium in the generation of bladder symp-

toms in interstitial cystitis/overactive bladder, urethral syndrome, prostatitis and gynaecological chronic pelvic pain. BJU Int 2011; 107: 370-5.
[15] Parsons CL. Diagnosing the bladder as the source of pelvic pain: successful treatment for adults and children. Pain Manag 2014; 4: 293-301.
[16] Parsons CL, Lilly JD and Stein P. Epithelial dysfunction in nonbacterial cystitis (interstitial cystitis). J Urol 1991; 145: 732-5.
[17] Buffington CA and Woodworth BE. Excretion of fluorescein in the urine of women with interstitial cystitis. J Urol 1997; 158: 786-9.
[18] Towner RA, Wisniewsky AB, Wu DH, Van Gordon SB, Smith N, North JC, McElhaney R, Aston CE, Shobeiri SA, Kropp BP, Greenwood-Van Meerveld B and Hurst RE. A feasibility study to determine whether clinical contrast-enhanced MRI can detect increased bladder permeability in patients with interstitial cystitis. J Urology 2016; 193: 631-8.
[19] Hurst RE, Moldwin RM and Mulholland SG. Bladder defense molecules, urothelial differentiation, urinary biomarkers, and interstitial cystitis. Urology 2007; 69: 17-23.
[20] Peter S. The junctional connections between the cells of the urinary bladder in the rat. Cell Tissue Res 1978; 187: 439-48.
[21] Hu P, Deng FM, Liang FX, Hu CM, Auerbach AB, Shapiro E, Wu XR, Kachar B and Sun TT. Ablation of uroplakin III gene results in small urothelial plaques, urothelial leakage, and vesicoureteral reflux. J Cell Biol 2000; 151: 961-72.
[22] Hurst RE, Van Gordon S, Tyler K, Kropp B, Towner R, Lin H, Marentette JO, McHowat J, Mohammedi E and Greenwood-Van Meerveld B. In the absence of overt urothelial damage, chondroitinase ABC digestion of the GAG layer increases bladder permeability in ovariectomized female rats. Am J Physiol Renal Physiol 2016; 310: F1074-80.
[23] Hauser PJ, VanGordon SB, Seavey J, Sofinowski TM, Ramadan M, Abdullah S, Buffington CA and Hurst RE. Abnormalities in expression of structural, barrier and differentiation related proteins, and chondroitin sulfate in feline and human interstitial cystitis. J Urol 2015; 194: 571-77.
[24] Zocher F, Zeidel ML, Missner A, Sun TT, Zhou G, Liao Y, von Bodungen M, Hill WG, Meyers S, Pohl P and Mathai JC. Uroplakins do not restrict CO2 transport through urothelium. J Biol Chem 2012; 287: 11011-7.
[25] Zupančič D, Romih R, Robenek H, Žužek Rožman K, Samardžija Z, Kostanjšek R and Kreft ME. Molecular ultrastructure of the urothelial surface: insights from a combination of various microscopic techniques. Microsc Res Tech 2014; 77: 896-901.
[26] Woodman JR, Mansfield KJ, Lazzaro VA, Lynch W, Burcher E and Moore KH. Immunocytochemical characterization of cultures of human bladder mucosal cells. BMC Urol 2011; 11: 5.
[27] Slobodov G, Feloney M, Gran C, Kyker KD, Hurst RE and Culkin DJ. Abnormal expression of molecular markers for bladder impermeability and differentiation in the urothelium of patients with interstitial cystitis. J Urol 2004; 171: 1554-8.
[28] Janssen DA, van Wijk XM, Jansen KC, van Kuppevelt TH, Heesakkers JP and Schalken JA. The distribution and function of chondroitin sulfate and other sulfated glycosaminoglycans in the human bladder and their contribution to the protective bladder barrier. J Urol 2013; 189: 336-42.
[29] Damiano R and Cicione A. The role of sodium hyaluronate and sodium chondroitin sulphate in the management of bladder disease. Ther Adv Urol 2011; 3: 223-32.
[30] Lucon M, Martins JR, Leite KR, Soler R, Nader HB, Srougi M and Bruschini H. Evaluation of the metabolism of glycosaminoglycans in patients with interstitial cystitis. Int Braz J Urol 2014; 40: 72-9.
[31] Saban R, Saban MR, Maier J, Fowler B, Tengowski M, Davis CA, Wu XR, Culkin DJ, Hauser P, Backer J and Hurst RE. Urothelial expression of neuropilins and VEGF receptors in control and interstitial cystitis patients. Am J Physiol Renal Physiol 2008; 295: F1613-23.
[32] Saban MR, Davis CA, Avelino A, Cruz F, Maier J, Bjorling DE, Sferra TJ, Hurst RE and Saban R. VEGF signaling mediates bladder neuroplasticity and inflammation in response to BCG. BMC Physiol 2011; 11: 16.
[33] Montalbetti N, Rued AC, Clayton DR, Ruiz WG, Bastacky SI, Prakasam HS, Eaton AF, Kullmann FA, Apodaca G and Carattino MD. Increased urothelial paracellular transport promotes cystitis. Am J Physiol Renal Physiol 2015; 309: F1070-81.
[34] Towner RA, Smith N, Saunders D, Van Gordon SB, Wisniewsky AB, Tyler KR, Greenwood-Van Meerveld B and Hurst RE. Contrast-enhanced magnetic resonance imaging (MRI) as a diagnostic tool for assessing bladder permeability and associated colon cross-talk: pre-clinical studies in a rat model. J Urology 2015; 193: 1394-400.
[35] He T, Smith N, Saunders D, Pittman BP, Lerner M, Lightfoot S, Silasi-Mansat R, Lupu F and Towner RA. Molecular MRI differentiation of VEGF receptor-2 levels in C6 and RG2 glioma models. Am J Nucl Med Mol Imaging 2013; 3: 300-311.
[36] de Souza PC, Smith N, Pody R, He T, Njoku C, Silasi-Mansat R, Lupu F, Meek B, Chen H, Dong

Y, Saunders D, Orock A, Hodges E, Colijn S, Mamedova N and Towner RA. OKN-007 decreases VEGFR-2 levels in a preclinical GL261 mouse glioma model. Am J Nuclear Med Mol Imaging 2015; 5: 363-78.

[37] Towner RA, Smith N, Doblas S, Garteiser P, Watanabe Y, He T, Saunders S, Herlea O, Silasi-Mansat R and Lupu F. In vivo detection of inducible nitric oxide synthase (iNOS) in rodent gliomas. Free Radic Biol Med 2010; 48: 691-703.

[38] Towner RA, Smith N, Saunders D, Lupu F, Silasi-Mansat R, West M, Ramirez DC, Gomez-Mejiba SE, Bonini MG, Mason RP, Ehrenshaft M and Hensley K. In vivo detection of free radicals using molecular MRI and immuno-spin-trapping in a mouse model for amyotrophic lateral sclerosis (ALS). Free Radic Biol Med 2013; 63: 351-360.

[39] Towner RA, Garteiser P, Bozza F, Smith N, Saunders D, d'Avila JCP, Magno F, Oliveira MF, Ehrenshaft M, Lupu F, Silasi-Mansat R, Ramirez DC, Gomez-Mejiba SE, Mason RP and Castro Faria-Neto HC. In vivo detection of free radicals in mouse septic encephalopathy using molecular MRI and immuno-spin-trapping. Free Radic Biol Med 2013; 65: 828-837.

[40] Coutinho de Souza P, Smith N, Atolagbe O, Ziegler J, Nijoku C, Lerner M, Ehrenshaft M, Mason RP, Meek B, Plafker SM, Saunders D, Mamedova N and Towner RA. OKN-007 decreases free radicals levels in a preclinical F98 rat glioma model. Free Radic Biol Med 2015; 87: 157-168.

[41] Towner RA, Smith N, Saunders D, De Souza PC, Henry L, Lupu F, Silasi-Mansat R, Ehrenshaft M, Mason RP, Gomez-Mejiba SE and Ramirez DC. Combined molecular MRI and immuno-spin-trapping for in vivo detection of free radicals in orthotopic mouse GL261 gliomas. Biochim Biophys Acta 2013; 1832: 2153-2161.

[42] Towner RA, Smith N, Saunders D, Carrizales J, Lupu F, Silasi-Mansat R, Ehrenshaft M and Mason RP. In vivo targeted molecular magnetic resonance imaging of free radicals in diabetic cardiomyopathy within mice. Free Radic Res 2015; 49: 1140-46.

[43] Towner RA, Smith N, Saunders D, Henderson M, Downum K, Lupu F, Silasi-Mansat R, Ramirez DC, Gomez-Mejiba SE, Bonini MG, Ehrenshaft M and Mason RP. In vivo imaging of immune-spin trapped radicals with molecular MRI in a mouse diabetes model. Diabetes 2012; 61: 2405-13.

[44] Dafni H, Landsman L, Schechter B, Kohen F and Neeman M. MRI and fluorescence microscopy of the acute vascular response to VEGF165: vasodilation, hyper-permeability and lymphatic uptake, followed by rapid inactivation of the growth factor. NMR Biomed 2002; 15: 120-31.

[45] Hermanson GT. Bioconjugate Techniques. San Diego: Academic Press; 1996. pp. 173-176.

[46] de Souza PC, Balasubramanian K, Njoku C, Smith N, Gillespie DL, Schwager A, Abdullah O, Ritchey JW, Fung KM, Saunders D, Jensen RL and Towner RA. OKN-007 decreases tumor necrosis and tumor cell proliferation and increases apoptosis in a preclinical F98 rat glioma model. J Magn Reson Imaging 2015; 42: 1582-91.

[47] Burgu B, McCarthy LS, Shah V, Long DA, Wilcox DT and Woolf AS. Vascular endothelial growth factor stimulates embryonic urinary bladder development in organ culture. BJU Int 2006; 98: 217-25.

[48] Montalbetti N, Rooney JG, Rued AC and Carattino MD. Molecular determinants of afferent sensitization in a rat model of cystitis with urothelial barrier dysfunction. J Neurophysiol 2019; 122: 1136-1146.

[49] Montalbetti N, Stocker SD, Apodaca G, Bastacky SI and Carattino MD. Urinary K+ promotes irritative voiding symptoms and pain in the face of urothelial barrier dysfunction. Sci Rep 2019; 9: 5509.

[50] Montalbetti N, Rued AC, Taiclet SN, Birder LA, Kullmann FA and Carattino MD. Urothelial tight junction barrier dysfunction sensitizes bladder afferents. eNeuro 2017; 4.